

# PEDOT quality: Another key factor determining the thermal stability of organic solar cells

Jingyuan Yao,<sup>1,‡</sup> Yuting Diao,<sup>1,‡</sup> Yanzhuo Zhu,<sup>1,‡</sup> Xiaojing Xu,<sup>1</sup> Rongchen Fu,<sup>1</sup> Bowen Gao,<sup>1</sup>

Huaxiang Xiang,<sup>1</sup> Xunchang Wang<sup>2</sup> and Yuda Li<sup>1\*</sup>

<sup>1</sup>Key Laboratory of Novel Biomass-based Environmental and Energy Materials in Petroleum and  
Chemical Industry, Key Laboratory for Green Process of Ministry of Education, School of  
Chemical Engineering and Pharmacy, Wuhan Institute of Technology, Wuhan, 430205, China. *E-*

*mail:* psydli@wit.edu.cn

<sup>2</sup>Key Laboratory of Optoelectronic Chemical Materials and Devices (Ministry of Education),  
School of Optoelectronic Materials & Technology, Jiangnan University, Wuhan 430056, China.

<sup>‡</sup>Jingyuan Yao, Yuting Diao and Yanzhuo Zhu contributed equal to this work.

## 1. Experimental Section

### 1.1 Materials

PSS with  $M_w$  of 200KDa were purchased from Sigma-Aldrich. EDOT monomer was purchased from Sigma-Aldrich. Ammonium persulfate (APS),  $FeCl_3$ , ethanediamine reducing agent and organic solvents including acetone, isopropanol, chloroform and methanol were purchased from Sinopharm Chemical and used without further purification. PM6, BTP-eC9 and PDINN were purchased from Solarmer Material Inc.

### 1.2 Synthesis of P-series PEDOT:PSSs

A typical protocol for the synthesis of P-series PEDOT:PSS is as follows: The PSS powder was added to 30 mL of deionized water, followed by the addition of EDOT

monomer under slow stirring conditions for 60 minutes. The pH was then adjusted to 1. Subsequently, APS was added with high-speed stirring (800 rpm). The feed mass ratio of EDOT to PSS is 1:8, while the mole ratio of APS to EDOT is set at 1.5:1. The above mixture was stirred at room temperature for a duration of 72 h and subsequently subjected to dialysis using a membrane with a molecular weight cutoff of 1000 Da for a period of 5 days. Finally, the PEDOT aqueous dispersion was concentrated to a mass concentration of 1.3% through the process of rotary evaporation. By varying the FeCl<sub>3</sub> content, P-0, P-1, P-20, P-50, and P-100 PEDOT:PSS products were synthesized.

### **1.3 Preparation of dedoped PEDOT:PSSs**

A typical dedoping protocol is shown as follows: PEDOT:PSS aqueous dispersion (100  $\mu$ L, 1.3 wt%) was added into 4 mL of deionized water. Then NaOH solution (500  $\mu$ L, 6 M) was added, followed by ethanediamine (100  $\mu$ L) under vivid stirring. Subsequently, the mixture was stirred at room temperature for 30 min. Finally, an azure aqueous dispersion of completely dedoped PEDOT:PSS was obtained.

### **1.4 Measurements and characterizations**

UV-vis-NIR absorption and transmittance spectra were recorded on a UV-3100 UV-vis spectrophotometer. XPS and UPS tests were conducted on a Thermo Scientific ESCALAB 250Xi instrument. AFM measurements were performed using Park XE-100 instrument by tapping mode. GIWAXS patterns were recorded on a Xeuss 3.0 Xenocs X-ray scattering instrument. Conductive devices with configuration of ITO/PEDOT:PSS sample/Al were fabricated with the following steps. Firstly, PEDOT:PSS aqueous dispersion was spin-coated onto clean ITO substrate and annealed at 150°C for 15 min. Then, the samples were transferred into the N<sub>2</sub>-filled glovebox. Finally, aluminum (100 nm) was thermally evaporated at about  $5 \times 10^{-4}$  Pa. *I-V* curves were detected in a glovebox by a Keithley 2420 source measurement unit under dark. The film thicknesses of P-0, P-1, P-20, P-50 and P-100 PEDOT:PSS films are 21, 23, 26, 25 and 28 nm, respectively. The in-plane conductivity tests were conducted according to the methodology described by Zhou et al.<sup>[1]</sup> Contact angle studies were carried out on a JC2000C1 static contact angle instrument. The  $\gamma_s$  values

of active layer materials were estimated by the surface wettability-based Owens–Wendt method. The Flory–Huggins interaction parameter  $\chi$  was obtained from the equation of  $\chi = K(\sqrt{\gamma_{donor}} - \sqrt{\gamma_{acceptor}})^2$ , where K is a constant.

### 1.5 OSCs fabrication and characterization

OSCs were fabricated as a layer stack of ITO/P-series PEDOT:PSSs/PM6:BTP-eC9/PDINN/Ag. Firstly, the ITO glass substrates were sequentially sonicated in detergent solution, deionized water, acetone, and isopropanol. Then, the substrates were further dried with nitrogen flow and subjected to an oxygen plasma treatment step for 8 min. Next, P-0 PEDOT:PSS (or P-1, P-20, P-50, P-100) aqueous dispersion was spin-coated onto the substrate and then annealed at 150 °C for 15 min. PM6:BTP-eC9 (ratio 1:1.2, 16.5 mg mL<sup>-1</sup> in chloroform, 0.5 vol% 1,8-diiodooctane additive) was then spin-coated at 3000 rpm for 30 s. PM6:BTP-eC9 film was annealed at 85 °C for 5 min. The film thicknesses of active layers are 100 nm. Subsequently, PDINN (1 mg mL<sup>-1</sup> in methanol) was spin-coated at 3000 rpm for 30 s and the film thickness is 8 nm. Finally, Ag was thermally evaporated at about 5 × 10<sup>-4</sup> Pa. The device area is 0.045 cm<sup>2</sup>.

*J–V* characteristics were detected in a glovebox by a Keithley 2450 source measurement unit under 100 mW cm<sup>-2</sup> (AM 1.5 G) irradiation. Light-intensity dependence measurements were recorded using the same instrument. Hole-only devices were fabricated with a device configuration of ITO/PEDOT:PSS/PM6:BTP-eC9/MoO<sub>3</sub>/Ag. The charge carrier mobility was determined by fitting the dark current to the model of a single carrier SCLC according to the equation:  $J = 9\varepsilon_0\varepsilon_r\mu V^2/8d^3$ , where *J* is the current density, *d* is the film thickness of the active layer,  $\mu$  is the charge carrier mobility,  $\varepsilon_r$  is the relative dielectric constant of the transport medium, and  $\varepsilon_0$  is the permittivity of free space.  $V = V_{app} - V_{bi}$ , where  $V_{app}$  is the applied voltage,  $V_{bi}$  is the built-in voltage.<sup>[2]</sup> The carrier mobility is calculated from the slope of the  $J^{1/2} \sim V$  curves. The  $P_{diss}$  values of OSCs were determined by calculating the  $J_{ph}/J_{sc}$  value at  $V_{eff} = 4$  V in the  $J_{ph}-V_{eff}$  curves. sEQE and EL measurements were performed following the method reported by Sun et al.<sup>[3]</sup> TPC and TPV measurements

were conducted on the PAIOS platform, which includes the characterization of solar cells and OLED.<sup>[4]</sup>

## 2. Supplementary figures and tables

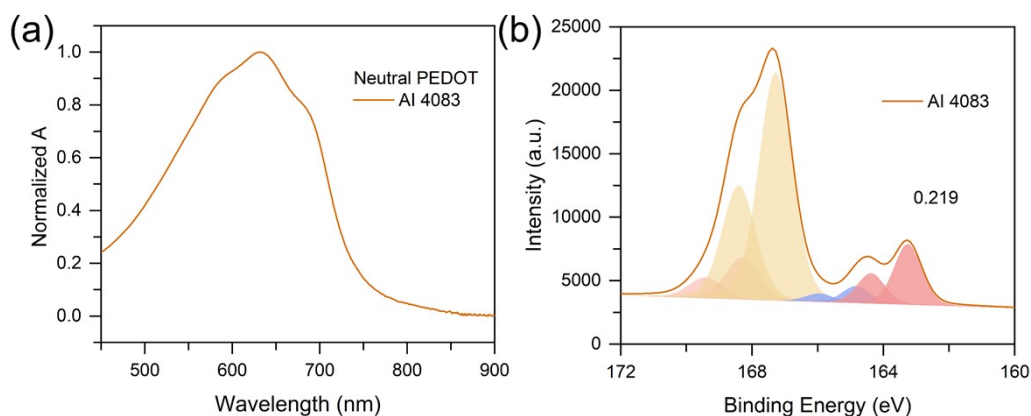


**Figure S1** (a) vis-NIR spectra of dedoped AI 4083 PEDOT:PSS aqueous dispersion. (b) XPS S2p spectrum of AI 4083 PEDOT:PSS film.

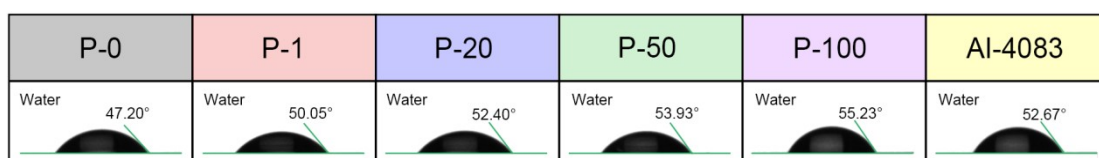


**Figure S2** Contact angles of water droplets on P-series and AI 4083 PEDOT:PSS films.

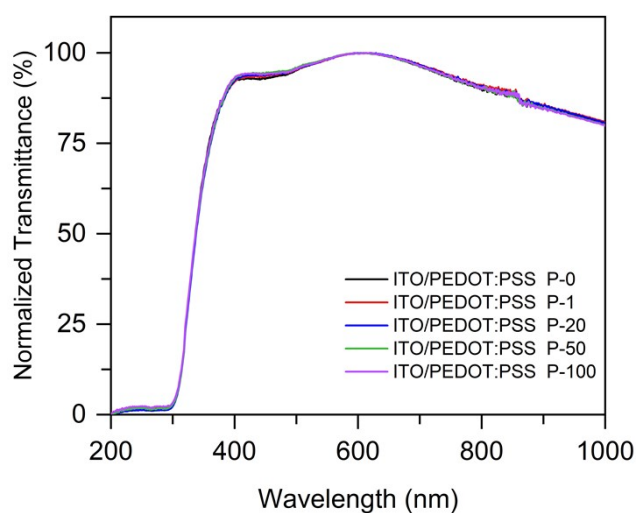


**Figure S3** Transmittance spectra of P-series PEDOT:PSS films deposited on ITO substrates.

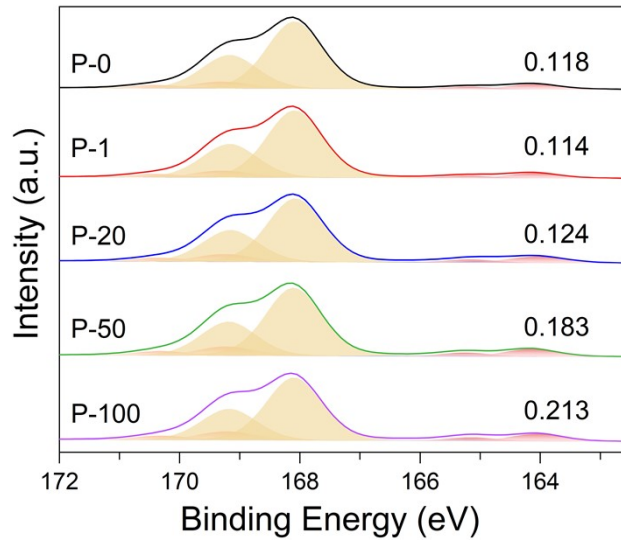


**Figure S4** XPS S2p spectrum of thermally aged P-series PEDOT:PSS films.

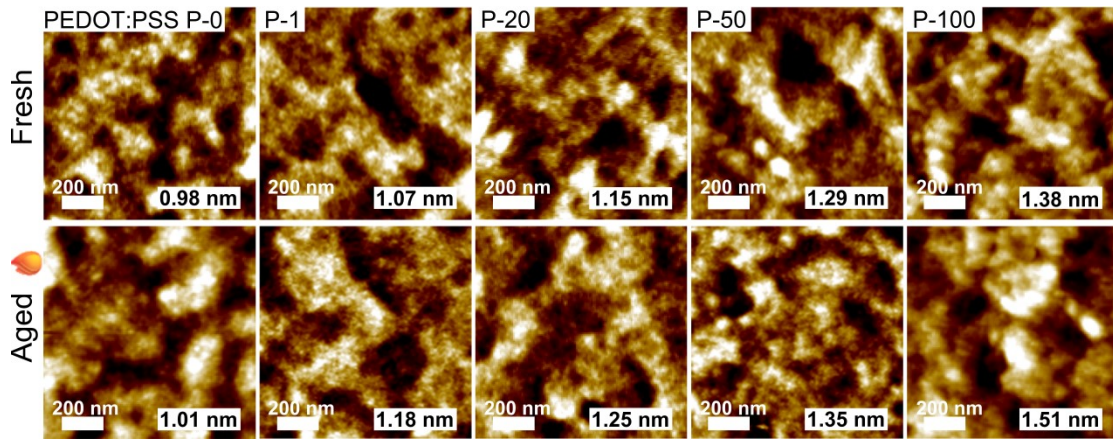


**Figure S5** AFM height images of freshly prepared and thermally aged PEDOT:PSS films.

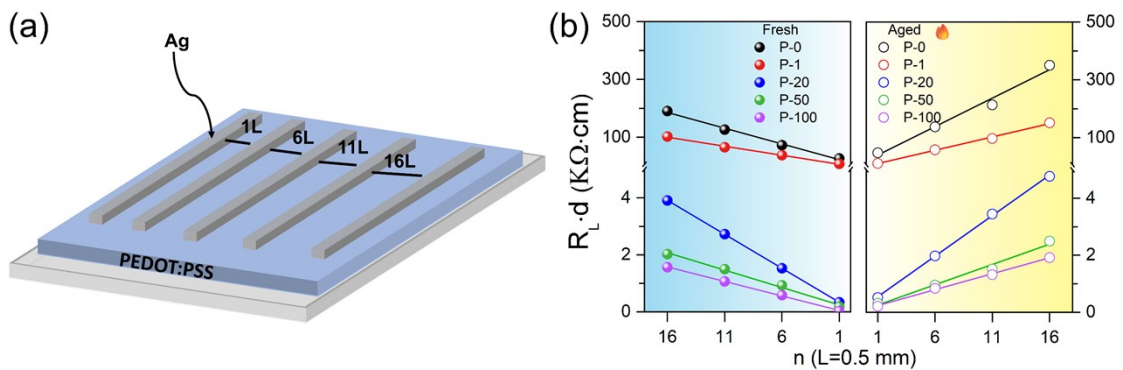


**Figure S6** (a) Schematic structure of the transmission line method for conductivity measurement. (b) Measured resistance of films as a function of channel length, and fit slope for conductivity calculation. Slope of the line is the resistance with a channel

length of  $L$  ( $R_L$ ,  $R_L = \Delta R/\Delta n$ ). The in-plane conductivity ( $\sigma_{\parallel}$ ) can be evaluated by the following equation:<sup>[1]</sup>  $\sigma_{\parallel} = L/(adR_L)$ , where  $L$  and  $a$  are the length and width of films;  $d$  denotes the film thickness.

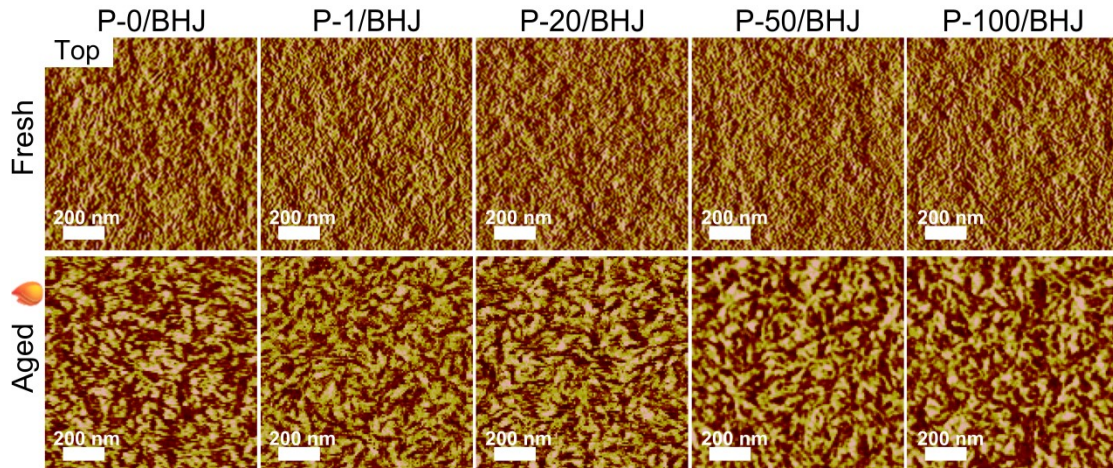


**Figure S7** AFM phase images of the top surfaces of freshly prepared and thermally aged PMT:BTP-eC9 films.

(a)	P-0/PM6 (~55 nm) $\gamma_s=35.34$ mN/m	P-1/PM6 (~55 nm) $\gamma_s=34.73$ mN/m	P-20/PM6 (~55 nm) $\gamma_s=34.98$ mN/m	P-50/PM6 (~55 nm) $\gamma_s=34.80$ mN/m	P-100/PM6 (~55 nm) $\gamma_s=34.56$ mN/m
	Water 96.2° 	Water 98.9° 	Water 101.5° 	Water 102.5° 	Water 106.3° 
	DIM 48.2° 	DIM 49.6° 	DIM 49.7° 	DIM 50.3° 	DIM 51.7° 
(b)	P-0/PM6 (~55 nm) $\gamma_s=33.69$ mN/m	P-1/PM6 (~55 nm) $\gamma_s=33.74$ mN/m	P-20/PM6 (~55 nm) $\gamma_s=33.59$ mN/m	P-50/PM6 (~55 nm) $\gamma_s=33.79$ mN/m	P-100/PM6 (~55 nm) $\gamma_s=33.64$ mN/m
	Water 89.4° 	Water 91.9° 	Water 91.8° 	Water 92.0° 	Water 92.7° 
	DIM 51.6° 	DIM 51.1° 	DIM 51.4° 	DIM 51.0° 	DIM 51.2° 
(c)	P-0/PM6 (~12 nm) $\gamma_s=34.52$ mN/m	P-1/PM6 (~12 nm) $\gamma_s=33.51$ mN/m	P-20/PM6 (~12 nm) $\gamma_s=33.04$ mN/m	P-50/PM6 (~12 nm) $\gamma_s=32.37$ mN/m	P-100/PM6 (~12 nm) $\gamma_s=32.03$ mN/m
	Water 88.9° 	Water 91.4° 	Water 95.4° 	Water 100.2° 	Water 100.5° 
	DIM 50.1° 	DIM 51.6° 	DIM 52.2° 	DIM 53.7° 	DIM 54.3° 
(d)	P-0/PM6 (~12 nm) $\gamma_s=36.70$ mN/m	P-1/PM6 (~12 nm) $\gamma_s=36.29$ mN/m	P-20/PM6 (~12 nm) $\gamma_s=35.99$ mN/m	P-50/PM6 (~12 nm) $\gamma_s=36.53$ mN/m	P-100/PM6 (~12 nm) $\gamma_s=36.08$ mN/m
	Water 89.9° 	Water 89.1° 	Water 89.6° 	Water 91.0° 	Water 89.8° 
	DIM 45.7° 	DIM 46.6° 	DIM 47.1° 	DIM 45.9° 	DIM 46.9° 

**Figure S8** Contact angles and  $\gamma_s$  values of (a,c) fresh and (b,d) aged PM6 films coated on various PEDOT:PSSs. The thick (~55 nm) and thin (~12 nm) films were employed to investigate the impact of PEDOT:PSS on the  $\gamma_s$  values of neighboring and distant PM6 molecules.

(a)	P-0/BTP-eC9 (~60 nm) $\gamma_s=42.48$ mN/m	P-1/BTP-eC9 (~60 nm) $\gamma_s=42.34$ mN/m	P-20/BTP-eC9 (~60 nm) $\gamma_s=42.21$ mN/m	P-50/BTP-eC9 (~60 nm) $\gamma_s=42.20$ mN/m	P-100/BTP-eC9 (~60 nm) $\gamma_s=41.78$ mN/m
	Water 90.2° 	Water 92.0° 	Water 92.2° 	Water 93.8° 	Water 96.2° 
	DIM 34.1° 	DIM 34.6° 	DIM 34.9° 	DIM 35.2° 	DIM 36.6° 
(b)	P-0/BTP-eC9 (~60 nm) $\gamma_s=42.32$ mN/m	P-1/BTP-eC9 (~60 nm) $\gamma_s=42.22$ mN/m	P-20/BTP-eC9 (~60 nm) $\gamma_s=42.09$ mN/m	P-50/BTP-eC9 (~60 nm) $\gamma_s=42.04$ mN/m	P-100/BTP-eC9 (~60 nm) $\gamma_s=42.12$ mN/m
	Water 89.8° 	Water 87.7° 	Water 89.8° 	Water 89.7° 	Water 88.2° 
	DIM 34.4° 	DIM 34.6° 	DIM 34.9° 	DIM 35.0° 	DIM 34.8° 
(c)	P-0/BTP-eC9 (~15 nm) $\gamma_s=54.39$ mN/m	P-1/BTP-eC9 (~15 nm) $\gamma_s=51.41$ mN/m	P-20/BTP-eC9 (~15 nm) $\gamma_s=46.95$ mN/m	P-50/BTP-eC9 (~15 nm) $\gamma_s=41.84$ mN/m	P-100/BTP-eC9 (~15 nm) $\gamma_s=39.63$ mN/m
	Water 50.8° 	Water 55.8° 	Water 62.7° 	Water 73.6° 	Water 80.9° 
	DIM 34.8° 	DIM 36.0° 	DIM 39.5° 	DIM 41.4° 	DIM 42.0° 
(d)	P-0/BTP-eC9 (~15 nm) $\gamma_s=49.52$ mN/m	P-1/BTP-eC9 (~15 nm) $\gamma_s=49.20$ mN/m	P-20/BTP-eC9 (~15 nm) $\gamma_s=50.06$ mN/m	P-50/BTP-eC9 (~15 nm) $\gamma_s=49.42$ mN/m	P-100/BTP-eC9 (~15 nm) $\gamma_s=50.27$ mN/m
	Water 57.1° 	Water 57.8° 	Water 56.9° 	Water 57.7° 	Water 56.5° 
	DIM 40.5° 	DIM 40.3° 	DIM 39.1° 	DIM 39.7° 	DIM 38.9° 

**Figure S9** Contact angles and  $\gamma_s$  values of (a,c) fresh and (b,d) aged BTP-eC9 films coated on various PEDOT:PSSs. The thick (~60 nm) and thin (~15 nm) films were employed to investigate the impact of PEDOT:PSS on the  $\gamma_s$  values of neighboring and distant BTP-eC9 molecules. The Flory–Huggins interaction parameter  $\chi$  was

obtained from the equation of  $\chi = K(\sqrt{\gamma_{donor}} - \sqrt{\gamma_{acceptor}})^2$ , where K is a constant. The calculated values of  $\chi$  were depicted in Figure 3b, c.

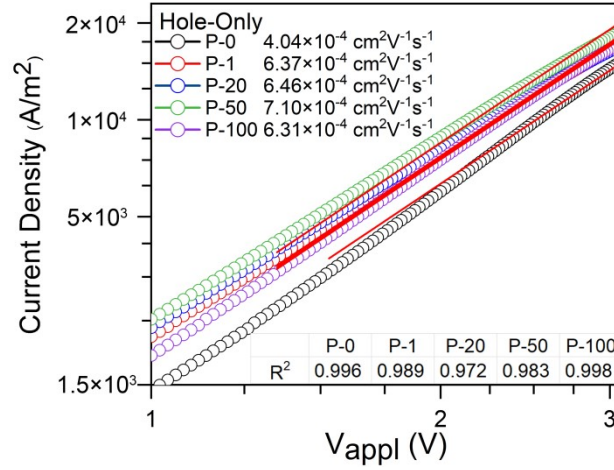


**Figure S10**  $J$ - $V$  curves of PM6:BTP-eC9 hole-only devices with different HTMs.

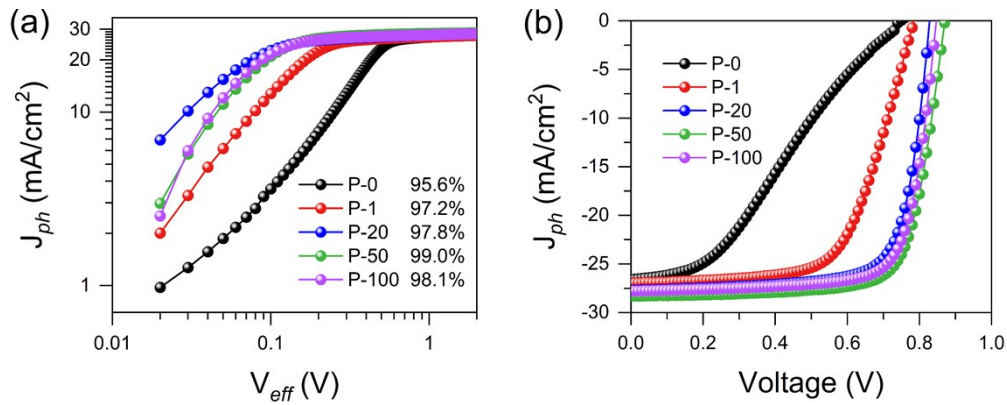


**Figure S11** (a)  $J_{ph}$ - $V_{eff}$  curves of OSCs. (b) The detail data of  $J_{ph}$ - $V$  curve with the bias voltage from 0 V to +1 V. The  $V_0$  values for P-0, P-1, P-20, P-50 and P100 devices are 0.75, 0.79, 0.83, 0.88 and 0.86 V, respectively.

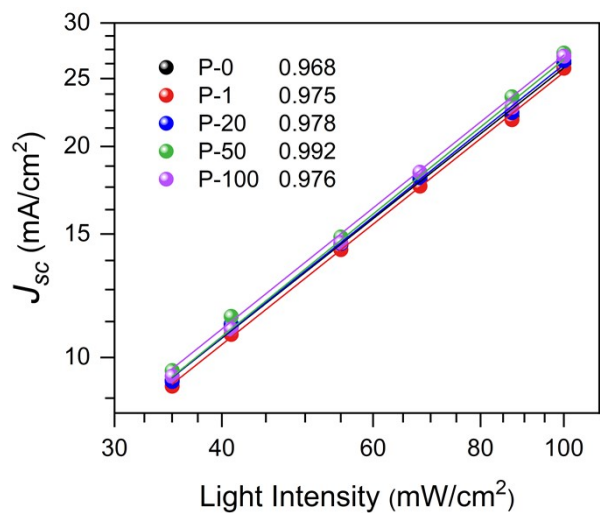


**Figure S12**  $J_{SC}$  versus light intensity of OSCs.

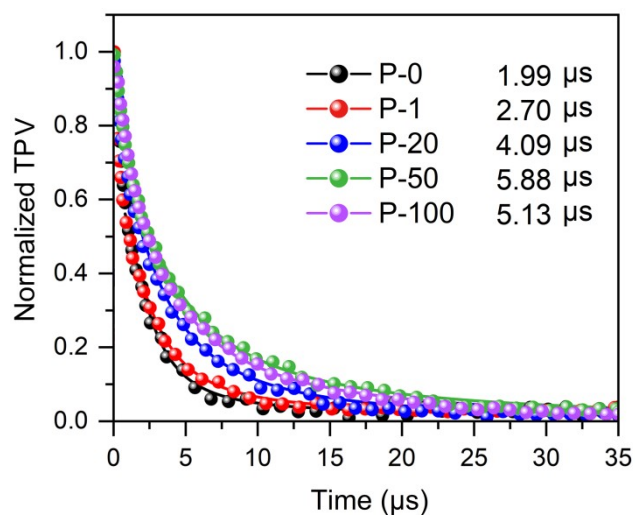


**Figure S13** TPV curves of OSCs.

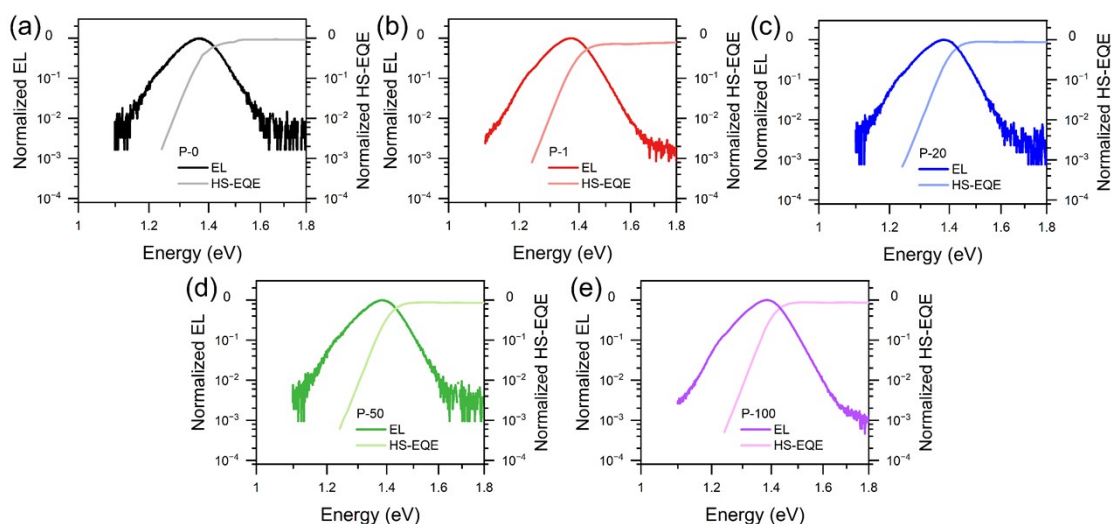


**Figure S14** Semi-logarithmic plots of the EL and sensitive EQE as a function of energy for (a) P-0, (b) P-1, (c) P-20, (d) P-50 and (e) P-100 OSCs.

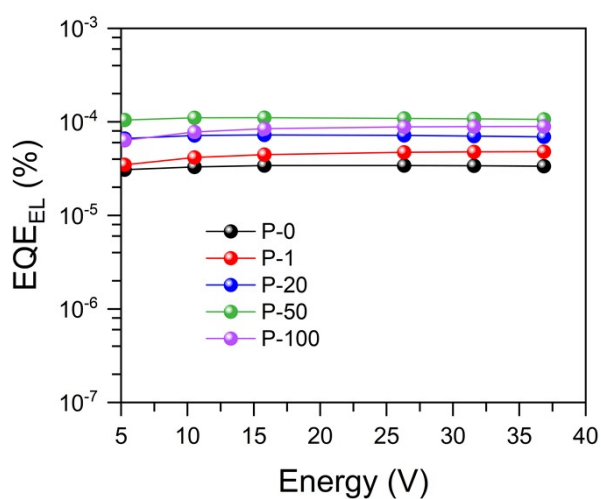


**Figure S15** EQE<sub>EL</sub> curves of the five OSCs.

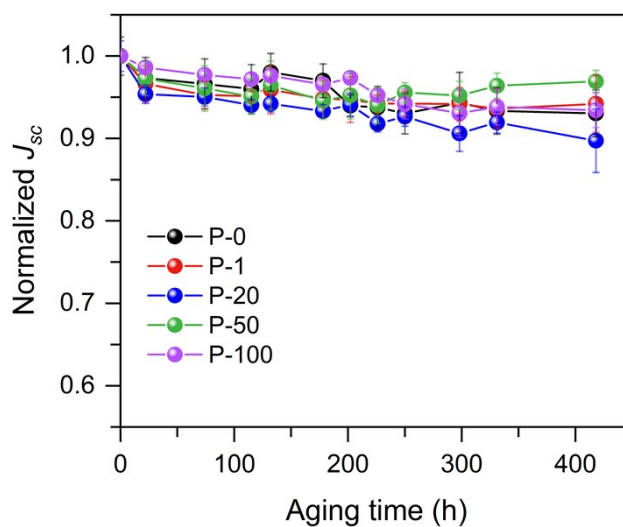


**Figure S16**  $J_{sc}$  evolution plots of OSCs in the stability test of thermal aging.

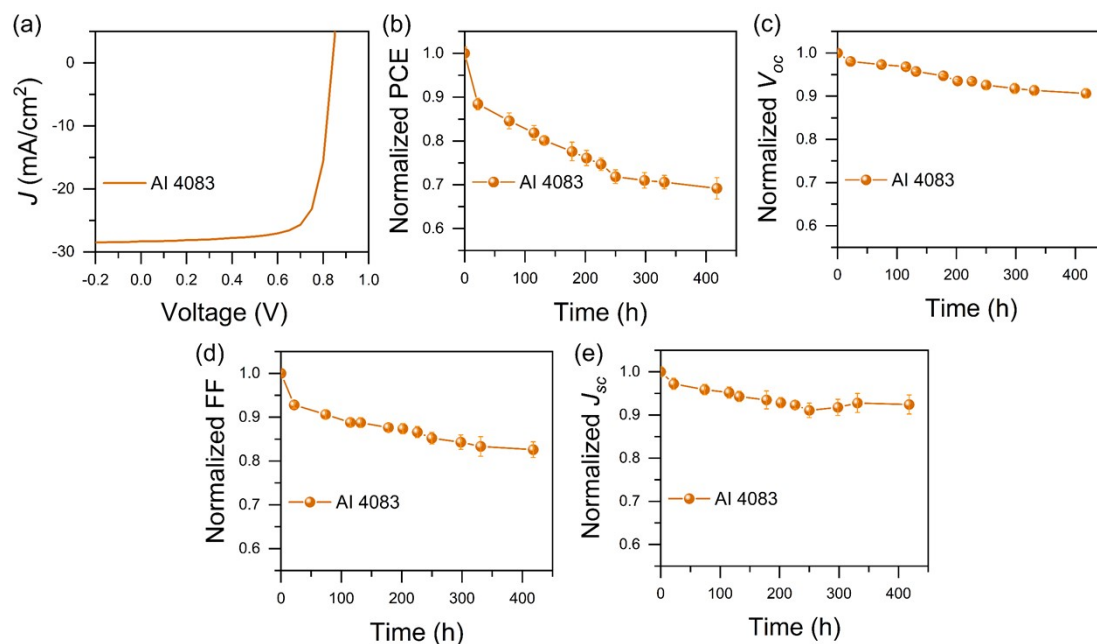


**Figure S17** (a)  $J$ - $V$  curves of 4083 OSC. (b) PCE, (c)  $V_{oc}$ , (d) FF and (e)  $J_{sc}$  evolution plots of 4083 OSC in the stability test of thermal aging.

[1] Jiang, Y., Dong, X., Sun, L., Liu, T., Qin, F., Xie, C., Jiang, P., Hu, L., Lu, X., Zhou, X., Meng, W., Li, N., Brabec, C.J. and Zhou, Y. An alcohol-dispersed conducting polymer complex for fully printable organic solar cells with improved stability. *Nature Energy*, 2022, 7(4), 352-359.

[2] Liu, T., Yang, T., Yang, T., Ma, R., Zhan, L., Luo, Z., Zhang, G., Li, Y., Gao, K., Xiao, Y., Yu, j., Zou, X., Sun, H., Zhang, M., Dela Peña, T.A., Xing, Z., Liu, H., Li, X., Li, G., Huang, J., Duan C., Wong, K., Lu, X., Guo, X., Gao, F., Chen, H., Huang, F., Li, Y., Li, Y., Cao, Y., Tang, B. and Yan, H. 16% efficiency all-polymer organic solar cells enabled by a finely tuned morphology via the design of ternary blend. *Joule*, 2021, 5(4), 914-930.

[3] Li, C., Zhou, J., Song, J., Xu, J., Zhang, H., Zhang, X., Guo, J., Zhu, L., Wei, D., Han, G., Min, J., Zhang, Y., Xie, Z., Yi, Y., Yan, H., Guo, F., Liu, F. and Sun, Y.

Non-fullerene acceptors with branched side chains and improved molecular packing to exceed 18% efficiency in organic solar cells. *Nature Energy*, 2021, 6(6), 605-613.

[4] Zhong, Z., Chen, S., Zhao, J., Xie, J., Zhang, K., Jia, T., Zhu, C., Jing, J., Liang, Y., Hong, L., Zhu, S., Ma, D. and Huang, F. Non-Halogen Solvent Processed Binary Organic Solar Cells with Efficiency of 19% and Module Efficiency Over 15% Enabled by Asymmetric Alkyl Chain Engineering. *Advanced Energy Materials*, 2023, 13(39), 202302273.